Deformation-Induced Martensite: A New Paradigm for Exceptional Steels

Soundes Djaziri, Yujiao Li, Gh. Ali Nematollahi, Blazej Grabowski, Shoji Goto, Christoph Kirchlechner, Aleksander Kostka, Stephen Doyle, Jörg Neugebauer, Dierk Raabe, and Gerhard Dehm**

Steel is the dominant structural engineering material with currently more than 1.6 billion tons produced every year.[1] Its enormous success is rooted in its wealth of properties, including ferromagnetism, high stiffness, corrosion resistance,[2,3] and, most importantly, its outstanding mechanical properties,[4–6] which can be extensively varied by manipulating the microstructure, making use of phase transformation and metastable phases. Among the various types of steel, plain carbon steels, i.e., Fe–C with minor additional alloying elements, are of a particular interest to the steel industry due to a good balance of properties and price. One of the most important phase transformation to harden plain carbon steels is the formation of martensite, a metastable Fe–C phase, which possesses a body-centered tetragonal (bct) structure.[7] Since its first observation by Martens using optical microscopy more than a century ago, it is metallurgical knowledge that two conditions must be satisfied to form Fe–C martensite: i) the carbon concentration needs to be sufficiently high, and ii) a rapid cooling of the steel from the high-temperature face-centered-cubic (fcc) austenite regime (γ-Fe) to very low temperatures must be applied. Based on more-recent studies[8,9] it is understood that martensite can be also mechanically induced from the austenite phase if the latter is retained in a metastable state after the quenching process. Here, we present the surprising discovery that Fe–C martensite can also be formed inside a pearlitic steel, i.e., a ferrite–cementite composite without any austenite, by a new and unexpected route: severe mechanical deformation.[10]

Current developments for improving the mechanical properties of metals, including steels, aim at producing nanostructured materials by severe plastic deformation (SPD).[11,12] To this end, cold-drawn pearlitic-steel wires have been very successful, reaching an ultrahigh tensile strength of up to ca. 7 GPa,[13] making them one of the world's strongest bulk materials. Pearlitic steels are used, for example, in large constructions such as suspension bridges. The high strength is associated with the refinement of the originally lamellar eutectoid body-centered-cubic (bcc) α-Fe (ferrite) + Fe_3C (cementite) structure of the pearlite, which leads to a nanocomposite that is stabilized by carbon segregation to the α-Fe grain boundaries.[13,14] With ongoing structure refinement, more and more carbon must be accommodated inside the ferrite due to the dissolution of the cementite.[15,16] As a consequence, the concentration of carbon in the α-Fe exceeds the equilibrium solubility limit by far. It is generally assumed that a high density of vacancies and dislocations[17] accommodate the excess carbon.[18–21] A recent study by Taniyama et al.,[22] revealed a tetragonal distortion of the ferrite lattice in heavily drawn pearlitic steel, which could be a consequence of the carbon supersaturation of the Fe matrix. Despite many studies on this topic, the accommodation of carbon in ferrite and a possible phase transformation are still controversial.

In this study, we have combined atom-probe tomography (APT) and synchrotron X-ray diffraction (XRD) to study the carbon supersaturation of ferrite for two pearlitic steel-wire compositions – eutectoid and hypereutectoid. Knowledge of the carbon accommodation in the ferrite provides control to design the strength and ductility of nanostructured pearlitic steels. True drawing strains, ε, of 0 to 6.52 were analyzed, exceeding by far the drawing strains studied previously.[22] The two compositions, the high strains, the combination of advanced chemical and structural characterization methods, and a supporting ab-initio-based theoretical description show that a new mechanism of martensite formation is triggered under the extreme deformation conditions that occur in the SPD-induced structural refinement of ultrahigh strength pearlitic steels. Deformation-driven nanoscale phase transformation provides a new way to tailor the mechanical properties of nanostructured steels and steel surfaces.

The synchrotron XRD results of the cold-drawn pearlitic-steel wires reveal significant microstructural changes induced by SPD. We focus on the evolution of the diffraction peaks of ferrite with drawing strain rather than on cementite decomposition. The four major diffraction peaks, {110}, {200}, {211} and

Dr. S. Djaziri, Dr. Y. Li, Dr. G. A. Nematollahi, Dr. B. Grabowski, Prof. S. Goto, Dr. C. Kirchlechner, Dr. A. Kostka,[+] Prof. J. Neugebauer, Prof. D. Raabe, Prof. G. Dehm
Max-Planck Institut für Eisenforschung
Max-Planck-Str. 1, D-40237 Düsseldorf, Germany
E-mail: djaziri@mpie.de; dehm@mpie.de

Prof. S. Goto
Department of Materials Science and Engineering
Faculty of Engineering and Resource Science
Akita University
Tegata Gakuencho Akita 010–8502, Japan

Dr. S. Doyle
Synchrotronstrahlungsquelle ANKA
Karlsruher Institut für Technologie (KIT)
Hermann-von-Helmholtz-Platz 1
76344 Eggenstein-Leopoldshafen, Germany

[+]Present address: Lehrstuhl Werkstoffdesign Institut für Werkstoffe Fakultät für Maschinenbau Ruhr-Universität Bochum, Universitätsstr. 150, 44780 Bochum, Germany

DOI: 10.1002/adma.201601526

{220}, of the initial wires are close to those of the undistorted bcc α-Fe phase. Noticeably, the {110} and {220} peaks shift to higher diffraction angles, whereas the {200} and {211} peaks slightly shift to lower values. The diffraction peaks were each decomposed into two sub-peaks so that the lattice parameters along the two different axes (a and c axes) could be extracted by applying the Bragg equation for both hypereutectoid and eutectoid wires. The analysis of the XRD ferrite peaks surprisingly reveals a deviation from the bcc lattice ($a = b = c$) for $\varepsilon \geq 2$ due to a tetragonal distortion ($a = b \neq c$), as shown in **Figure 1**a. The effect increases with larger drawing strain as shown by the c/a ratio (Figure 1b). This observation holds true for both eutectoid and hypereutectoid compositions. Figure 1a reveals three stages in the evolution of the lattice parameter with drawing strain. In the first stage, the ferrite unit cell has a bcc crystal structure where the lattice parameter remains unchanged and is equal to that of pure iron. At $\varepsilon = 2$, the lattice parameter splits into two values corresponding to a tetragonal structure with two different axes a and c. Up to $\varepsilon = 4$, the a-axis shrinks by ca. 0.36%, while the c-axis expands by ca. 0.45%. At even higher strains, the lattice parameter values a and c remain constant within experimental error. Interestingly, the volume of the unit cell of the α-Fe phase remains unchanged during the drawing process although a tetragonal distortion occurs.

To better understand the origin of the observed tetragonal distortion, we revisited published data on the relationship between the distorted lattice parameters and the carbon content.[24,25] However, rather than using the nominal bulk alloy carbon content, we conducted APT studies to quantitatively determine the fraction of the solute carbon content within the α-Fe grain interiors for wires at several drawing strains. Figure 1c summarizes the measured carbon concentration versus the drawing strain for both nominal compositions. It can be seen that more carbon atoms are released into the ferrite at $\varepsilon = 5$ (0.58 ± 0.11 at%) than at $\varepsilon = 2$ (0.20 ± 0.05 at%), always exceeding the solubility limit of C in the α-Fe lattice.

We find that the drawing process induced a significant increase in the carbon content inside the originally near-carbon-free ferrite until a steady state is approached at drawing strains larger than ca. 4 for the wires (Figure 1c). The change of carbon concentration in the ferrite grains during the drawing process is closely related to the tetragonal distortion of the ferrite unit cell. Indeed, the bct structure of ferrite is stabilized in the third stage ($\varepsilon > 4$), which is attributed to the saturation of the carbon concentration in the ferrite grains. We note also that the c/a ratio reaches a steady state in the third stage where $c/a = 1.007 \pm 0.002$. This is an unexpected observation since tetragonal distortion of the ferrite due to solute carbon is usually observed from as-quenched martensite. Hence, the fundamental question arises as to whether severe plastic deformation can produce the same type of distorted phase via a completely different route, i.e., deformation-driven martensite rather than a diffusionless γ-Fe (austenite) $\rightarrow$ martensite phase transformation.

The literature suggests that the c/a ratio of the as-quenched bct martensite lattice depends on the carbon concentration according to the relationship $c/a = 1 + 0.045p$, where p is the carbon content in weight percent (wt%).[24,25] The tetragonal symmetry of an as-quenched martensite lattice is characterized by preferential carbon atom occupation of the octahedral

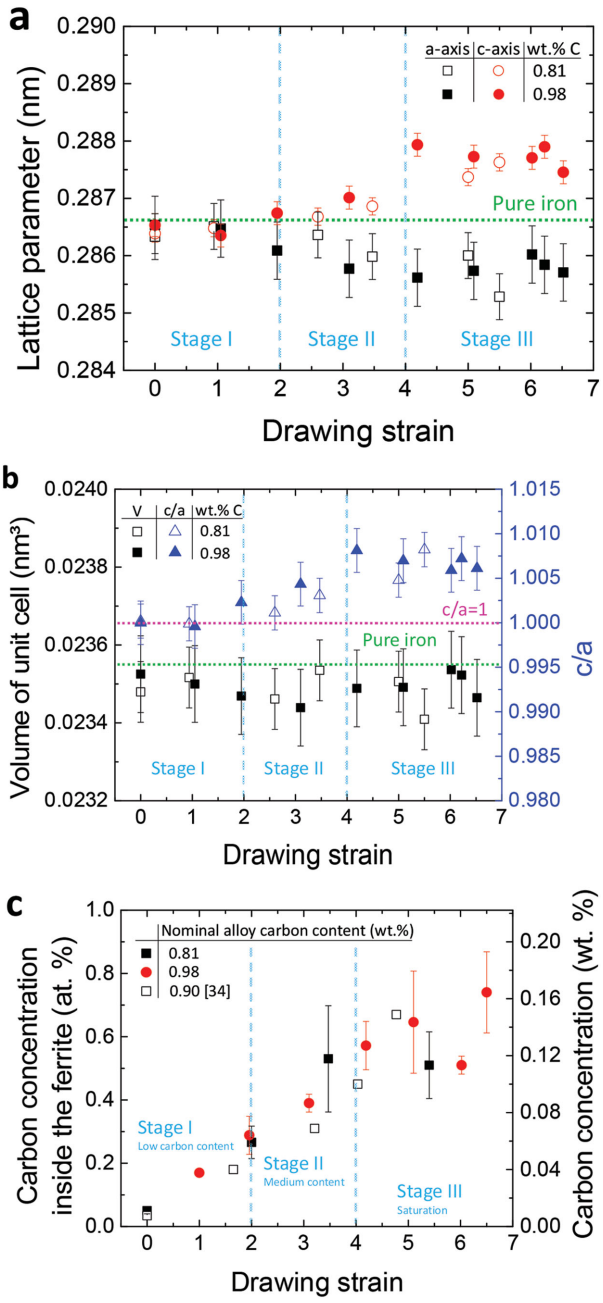

Figure 1. Structural evolution of ferrite, probed by XRD and APT. a) Lattice parameters along the a- and c-axis, b) unit-cell volume and c/a ratio of the α-ferrite lattice as functions of the drawing strain. The green dashed lines correspond to pure iron and the pink dashed line marks $c/a = 1$. The blue dashed lines highlight the different stages of structure evolution. c) Carbon concentration inside the ferrite grain interiors as observed by APT as a function of the wire drawing strain for pearlite wires with different nominal alloy carbon concentrations. Literature data.[23] for hypereutectoid (0.90 wt% C) pearlitic steel are used for comparison.

interstitial sites at ½ <100> along one of the three sublattices in the bcc α-iron lattice.[24,25] Thus, the tetragonal distortion (the c/a ratio) increases with increasing carbon content in the matrix. When using the average value of the c/a ratio from our current XRD data observed in the third stage, this translates

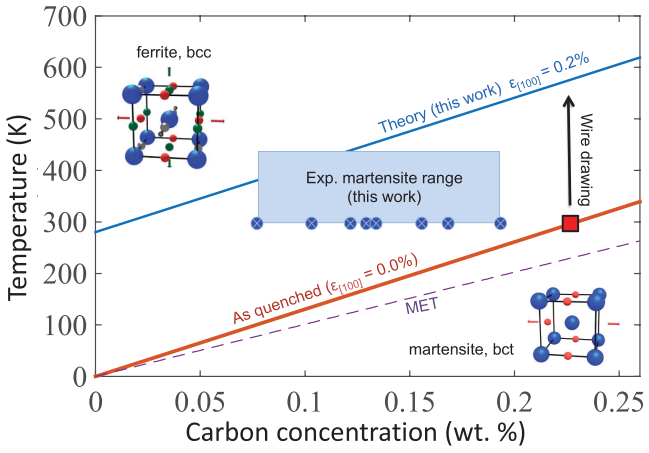

Figure 2. Predicted Fe–C equilibrium phase diagram obtained with the ab-initio-based model developed here. The order–disorder transformation temperatures are plotted as a function of carbon concentrations for 0.2% lattice strain (blue line) and in the absence of any strain (red line). The red square corresponds to the only available experimental data point for an as-quenched martensitic transformation.[30] The blue dots represent C concentrations of the tetragonally distorted martensite measured in this work. The dashed line represents the order-disorder transformation predicted by means of microscopic elasticity theory (MET).[24]

to a carbon concentration of 0.16 wt% causing the distortion, which is in good agreement with the APT data of 0.12 wt% C and 0.14 wt% C for the eutectoid and hypereutectoid wires, respectively (Figure 1c). This is consistent with previous studies reporting a supersaturation of carbon atoms in ferrite,[26–28] however, without noticing its tetragonal distortion. The XRD and APT results thus bring up the surprising question as to whether the martensite could have formed by the severe deformation alone without any preceding heat treatment and quenching.

The difference between a bcc and bct (martensite) crystal structure is the thermodynamic preference for ordering of carbon atoms within one interstitial sublattice of bcc. Zener pointed out that an indirect, strain-induced interaction between the carbon atoms causes this spontaneous ordering.[29] Based on Zener's work, Kurdjumov and Khachaturyan[24] developed a model for the order–disorder transition using microscopic elasticity theory (MET). However, the mechanically driven bcc–bct transition observed in our work cannot be explained by Khachaturyan's model (**Figure 2**), which is a thermodynamic concept that neglects the severe strains and strain inhomogeneity present in the wire.

We have therefore developed an approach that can also take into account lattice strains – which are caused by the externally applied strain (first order residual strains) or microstructural strain of second or third order. As shown in Figure 2 by the red line, the critical transition temperature at zero applied strain obtained from our new approach follows a similar trend as the MET model from Kurdjumov and Khachaturyan[24] and slightly extends the stability region of martensite, now matching the experimental data point for as-quenched martensite.[31,30] However, without any lattice strain, the deformation-induced martensite (blue dots) cannot be explained. As shown in Figure 2, even a small elastic lattice strain of 0.2% largely stabilizes the ordering of the carbon atoms in one of the octahedral sublattices, resulting in a significant upward shift of the transition temperature (blue line), moving all the experimental data points into the ordered stability regime, hence, confirming the experimental observations. While an exact determination of the elastic strain during wire drawing is not possible due to the highly complex geometry and microstructure, elastic strains up to 1% seem realistic. This can be estimated by noting that the total elastic strain applied by the wire drawing machine is $\varepsilon = \sigma/E$, where E is the Young's modulus and σ the yield stress. Since the Young's modulus is about 210 GPa and the yield stresses are 2–4 GPa, the total elastic strains (external as well as microstructural strain of second or third order) can reach values of 1–2%.

According to our findings two conditions must be fulfilled to create deformation-induced martensite: i) the bcc α-Fe must get supersaturated with carbon, and ii) sufficient lattice strains need to be present. The origin of the carbon supersaturation is closely linked to the deformation-driven cementite decomposition resolved in our study, as well as in several previous

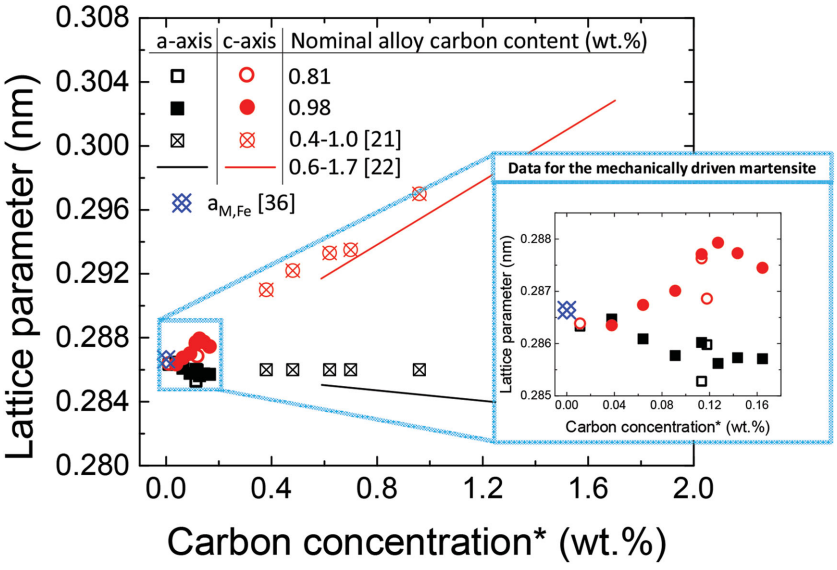

Figure 3. Comparison of results with literature data. The lattice parameters a and c of conventional as-quenched martensite with different nominal (i.e., global) alloy carbon content (cross symbols and solid lines) taken from the literature,[24,25] plotted together with the ferrite phase of the current heavily drawn wires at different true strains (C content) as determined in this study. Our data (open and filled symbols) extend the as-quenched martensite data[24,25] to lower C contents, indicating that wire drawing induces a martensite-like tetragonal distortion of the initial bcc Fe phase. A magnified plot of our data is shown in the inset. $a_{M,Fe}$ refers to the lattice parameter of martensite in carbon-free iron at room temperature, which is equivalent to the lattice parameter of ferrite.[38] The asterisk * on the abscissa axis has been added to underline the difference between the carbon content of the present study, which is measured by APT in the ferrite grain interiors, and the data taken from literature, which refer to the nominal alloy carbon content.

observations.[32–34] The decomposition of cementite is triggered by dislocations dragging carbon atoms out of the decomposing cementite due to a high binding energy between both (0.8 eV).[35] This results in a carbon-supersaturated Fe matrix and segregation of carbon atoms to grain boundaries stabilizing the nanosized Fe grain structure.[13,14,32,36] For the same samples, Li el al. reported a transition from a lamellar pearlite to a nanocrystalline microstructure during wire drawing at very high drawing strains.[13] The refinement in grain size leads to an increase in tensile strength following the Hall–Petch law. In contrast, the present study focuses on the accommodation of C in the Fe matrix. The tetragonality may contribute to the strength but as the wires approach the theoretical strength of steel, we believe that the nanoscale grain size is the strength-controlling mechanism. However, the loss in ductility may be triggered by the Fe–C martensite, which is known to be a brittle phase.

We also verified that the classical path of forming martensite by quenching from the austenite region can be excluded in our study. Although friction and plastic deformation during SPD may lead to temperature increases of up to 200 °C, no indication of austenite formation has ever been detected. In the case that local heating would have led to austenite formation, it would be unexpected that all the γ-Fe is transformed into martensite. This hypothesis can be excluded since, in the numerous SPD experiments on pearlitic steel, no retaining austenite has been observed. We can also exclude that a reverse transformation of ferrite to austenite, as reported by MacLaren et al.,[37] occurred in our sample, since no austenite was detected by XRD and transmission electron microscopy (TEM) (see Figure S2 and S3, Supporting Information)

Finally, we note that the structural parameters of the deformation-induced and the transformation-induced martensite are consistent. In **Figure 3**, we therefore compare the lattice parameters of martensite from the various studies compared with our current data.[24,25,38] The bct lattice parameters and carbon contents measured for our severely deformed wires fit with extrapolated lattice parameters of quenched-in martensite determined by Kurdjumov and Khachaturyan.[24] An even better agreement is obtained when extrapolating the data of Roberts.[25] These observations exhibit again a clear signature of the spontaneous ordering of carbon atoms on the octahedral interstitial sites, causing the ferrite unit cell to be tetragonally distorted.

In conclusion, the concept of deformation induced Fe–C martensite is general. It requires decomposition of a carbon-rich phase (like cementite), and deformation-induced carbon supersaturation of the initial bcc Fe matrix. This may be most easily achieved for pearlitic steels, but may also occur for severely deformed Bainite steels. However, for pearlitic steels, it is well known that the interlamellar spacing has a significant effect on cementite dissolution and the tensile strength of drawn wires.[39]

In summary, our findings reveal that cold-drawing of pearlitic steel wires leads to a carbon-supersaturated ferrite causing a spontaneous tetrag

onal distortion of the ferrite unit cell through a strain-induced deformation driven martensitic transformation. This hitherto unknown mechanism can be beneficial by increasing the strength of steels, but may also become detrimental when the deformation-induced martensite reduces the ductility and thus enhances crack initiation. An example would be pearlitic steels exposed to extreme deformations, such as in the contact region of railway tracks and wheels. Knowing this mechanism is crucial to overcome such failure mechanisms.

Experimental Section

The samples studied in this work are pearlitic steel wires of two types of composition: a eutectoid composition with 0.8 wt% C (provided by Nippon Steel Corporation) and a hypereutectoid composition with 0.98 wt% C (provided by Suzuki Metal Industry Co., Ltd). The complete chemical composition of the samples can be found in the Supporting Information. The samples were cold-drawn at different strains up to true drawing strains of $\varepsilon = 5.5$ and $\varepsilon = 6.52$ for the eutectoid steel and the hypereutectoid steel, respectively. The wire diameters range from 1.7 mm down to 0.058 mm for the eutectoid steel and from 0.54 mm down to 0.02 mm for the hypereutectoid steel. The highest total wire drawing strain ($\varepsilon = 6.52$) leads to a very high tensile strength of 7 GPa.[13]

Supporting Information

Supporting Information is available from the Wiley Online Library or from the author.

Acknowledgements

The authors would like to thank Suzuki Metal Industry Co., Ltd. and Nippon Steel Corporation, for providing the cold-drawn specimens. Moreover, the authors thank their colleagues at MPIE: Dr. V. Marx, B. Breitbach, Dr. J. Balila, and C. Fink for their great help during the synchrotron measurements at PDIFF/ANKA.

Received: March 18, 2016
Revised: May 17, 2016
Published online: July 4, 2016

[1] Stahl Online, Monatliche Welt-Rohstahlerzeugung, http://www.stahl-online.de/wp-content/uploads/2013/08/Welt_September2015_dt.png, accessed: September **2015**.
[2] M. J. Duarte, J. Klemm, S. O. Klemm, K. J. J. Mayrhofer, M. Stratmann, S. Borodin, A. H. Romero, M. Madinehei, D. Crespo, J. Serrano, S. S. A. Gerstl, P. P. Choi, D. Raabe, F. U. Renner, *Science* **2013**, *341*, 372.
[3] M. P. Ryan, D. E. Williams, R. J. Chater, B. M. Hutton, D. S. McPhail, *Nature* **2002**, *415*, 770.
[4] Y. Kimura, T. Inoue, F. Yin, K. Tsuzaki, *Science* **2008**, *320*, 1057.
[5] M. Taneike, F. Abe, K. Sawada, *Nature* **2003**, *424*, 294.
[6] L. Vitos, P. A. Korzhavyi, B. Johansson, *Nat. Mater.* **2003**, *2*, 25.
[7] R. Abbaschian, L. Abbaschian, R. E. Reed-Hill, *Physical Metallurgy Principles,* Cengage Learning, Stamford, CT, USA **2008**, Ch. 17.
[8] A. Molkeri, F. Pahlevani, I. Emmanuelawati, V. Sahajwalla, *Mater. Lett.* **2016**, *163*, 209.
[9] A. Litwinchuk, F. X. Kayser, H. H. Baker, A. Henkin, *J. Mater. Sci.* **1976**, *11*, 1200.
[10] The term Fe–C martensite is used in this context as a general notion to specify the tetragonal Fe crystal structure supersaturated with carbon and not alone the product of the displacive phase transformation of Fe–C austenite. In the current case, we reveal that these two states are indistinguishable.

[11] Y. Wang, M. Chen, F. Zhou, E. Ma, *Nature* **2002**, *419*, 912.
[12] R. Valiev, *Nat. Mater.* **2004**, *3*, 511.
[13] Y. J. Li, D. Raabe, M. Herbig, P.-P. Choi, S. Goto, A. Kostka, H. Yarita, C. Borchers, R. Kirchheim, *Phys. Rev. Lett.* **2014**, *113*, 106104.
[14] M. Herbig, D. Raabe, Y. J. Li, P. P. Choi, S. Zaefferer, S. Goto, *Phys. Rev. Lett.* **2014**, *112*, 126103.
[15] D. Raabe, P. P. Choi, Y. J. Li, A. Kostka, X. Sauvage, F. Lecouturier, K. Hono, R. Kirchheim, R. Pippan, D. Embury, *MRS Bull.* **2010**, *35*, 982.
[16] Y. Z. Chen, A. Herz, Y. J. Li, C. Borchers, P. P. Choi, D. Raabe, R. Kirchheim, *Acta Mater.* **2013**, *61*, 3172.
[17] Y. Z. Chen, G. Csiszár, J. Cizek, S. Westerkamp, C. Borchers, T. Ungár, S. Goto, F. Liu, R. Kirchheim, *Metall. Mater. Trans. A.* **2013**, *44A*, 3882.
[18] Y. Yamada, *Trans. Iron Steel Inst. Jpn.* **1976**, *16*, 417.
[19] V. G. Gavriljuk, *Mater. Sci. Eng.* **2003**, *A345*, 81.
[20] X. Sauvage, Y. Ivanisenko, *J. Mater. Sci.* **2007**, *42*, 1615.
[21] G. A. Nematollahi, B. Grabowski, D. Raabe, J. Neugebauer, *Acta Mater.* **2016**, *111*, 321.
[22] A. Taniyama, T. Takayama, M. Arai, T. Hamada, *Scr. Mater.* **2004**, *51*, 53.
[23] N. Maruyama, T. Tarui, H. Tashiro, *Scr. Mater.* **2002**, *46*, 599.
[24] G. V. Kurdjumov, A. G. Khachaturyan, *Acta Metall. Mater.* **1975**, *23*, 1077.
[25] C. S. Roberts, *Trans. AIME* **1953**, *197*, 203.
[26] K. Hono, *Scr. Mater.* **2001**, *44*, 977.
[27] D. E. Jiang, E. A. Carter, *Phys. Rev. B* **2003**, *67*, 214103.
[28] J. H. Jang, H. K. D. H. Bhadeshiaa, D. W. Suh, *Scr. Mater.* **2013**, *68*, 195.
[29] C. Zener, *Phys. Rev.* **1948**, *74*, 639.
[30] A. Udyansky, J. von Pezold, A. Dick, J. Neugebauer, *Phys. Rev. B.* **2011**, *83*, 184112.
[31] A. Udyansky, J. von Pezold, V. N. Bugaev, M. Friák, J. Neugebauer, *Phys. Rev. B.* **2009**, *79*, 224112.
[32] Y. J. Li, P. Choi, C. Borchers, S. Westerkamp, S. Goto, D. Raabe, R. Kirchheim, *Acta Mater.* **2011**, *59*, 3965.
[33] V. G. Gavriljuk, *Scr. Mater.* **2001**, *45*, 1469.
[34] F. Wetscher, R. Pippan, S. Sturm, F. Kauffmann, C. Scheu, G. Dehm, *Metall. Mater. Trans. A* **2006**, *37A*, 1963.
[35] L. Ventelon, B. Lüthi, E. Clouet, L. Proville, B. Legrand, D. Rodney, F. Willaime, *Phys. Rev. B* **2015**, *91*, 220102.
[36] Y. J. Li, A. Kostka, P. Choi, S. Goto, D. Ponge, R. Kirchheim, D. Raabe, *Acta Mater.* **2015**, *84*, 110.
[37] I. MacLaren, Y. Ivanisenko, R. Z. Valiev, H. J. Fecht, *J. Phys., Conf. Ser.* **2006**, *26*, 335.
[38] S. J. Lee, S. Lee, B. C. De Cooman, *Scr. Mater.* **2011**, *64*, 649
[39] W. J. Nam, C. M. Bae, S. J. Oh, S.-J. Kwon, *Scr. Mater.* **2000**, *42*, 457.